Supplement of Earth Surf. Dynam., 10, 875–894, 2022
https://doi.org/10.5194/esurf-10-875-2022-supplement

Supplement of

Drainage reorganization induces deviations in the scaling between valley width and drainage area

Elhanan Harel et al.

Correspondence to: Elhanan Harel (elhananh@post.bgu.ac.il)

S1 Algorithm for identifying optimal locations for width measurements

This section describes the semi-automatic ArcGIS-based algorithm for measuring valley width. The algorithm input is a valley bottom (VBET) polygon, and the output is a set of width measurement locations and values.

1. A network of valley centerlines is defined for the valley bottom polygon (Fig. S1) by applying the external ArcGIS tool ‘polygon to centerline’ (Dilts, 2015). Valley center points are distributed along the centerline at distances ranging between 5-20 m, in accordance with the basin size.

2. Thiessen (Voronoi) polygons are created around the centerline points and clipped based on the extent of the VBET polygon (Fig. S2A).

3. Intersecting edges of Thiessen polygons are eliminated (Fig. S2B). The remaining edges, which are sub-perpendicular to the centerlines, cross the VBET polygon from side to side, and are far from valley confluences and bends, are defined as ‘crossing Thiessen lines.’

4. Steps 2-3 are repeated twice more (overall three iterations). In each iteration, the centerlines are trimmed relative to the previous iteration, such that in each iteration, the minimal valley order (sensu Strahler) included in the centerline network is higher. The second and third iterations are designated to increase the number of ‘crossing Thiessen lines’ along the high order valleys: At the end of the first iteration, ‘crossing Thiessen lines’ are generated along valleys of all orders. In the second iteration, new ‘crossing Thiessen lines’ are generated only along second and higher order valleys, and so on in the third iteration. When a new ‘crossing Thiessen line’ intersects a ‘crossing Thiessen line’ generated in a previous iteration, the new line is eliminated. Finally, ‘crossing Thiessen lines’ from all three iterations are merged into a single shapefile (Fig. S3). In the current study, three iterations were sufficient to generate ‘crossing Thiessen lines’ in basins with high order valleys. However, future use of this method for basins with valley order >5 should consider additional iterations.

5. Centerline segments bounded between pairs of ‘crossing Thiessen lines’ that were adjacent to each other prior to step 3, are defined as ‘Width-locator segments,’ and their midpoints are marked (Fig. S4). Following, ’Width transects’ are generated perpendicular to the ‘width-locator segments.’ ’Width transects’ cross the midpoints and terminate at the edges of the valley bottom polygon (Fig. S4). ‘Width transects’ are generated by applying the external ArcGIS ‘Create perpendicular lines tool’ (Gabrish, 2020), and their length represent the local valley width (Fig. 3A).

7. Finally, the ‘intersection points’ between the ‘Width transects’ and the channel talweg (flowlines) are marked (Fig. S5). Drainage area and topographic data used for slope calculation are extracted at the ‘intersection points,’ based on the TanDEM-X 0.4 arcsec DEM (Wessel, 2016).

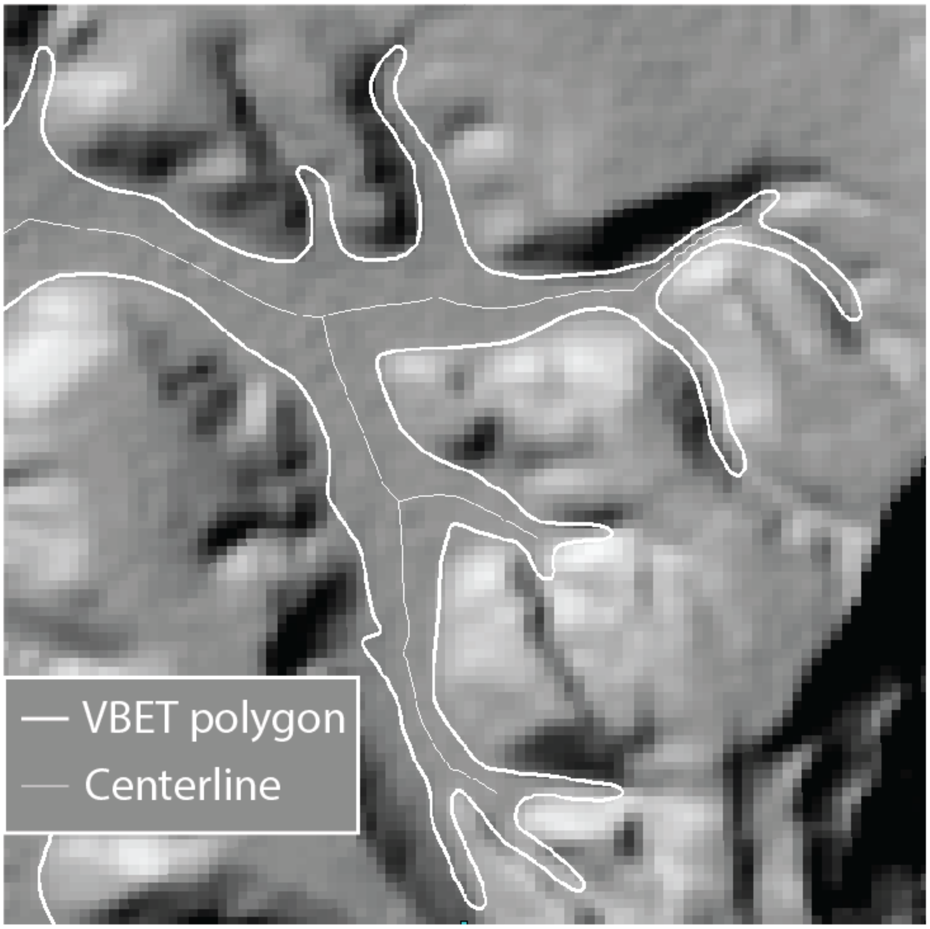

Figure S1. The VBET polygon (thick lines) and its centerline (thin lines). The current and following examples are based on the basin containing valley 4, and the hillshade backgrounds are based on TanDEM-X 0.4 arcsec DEM (Wessel, 2016)

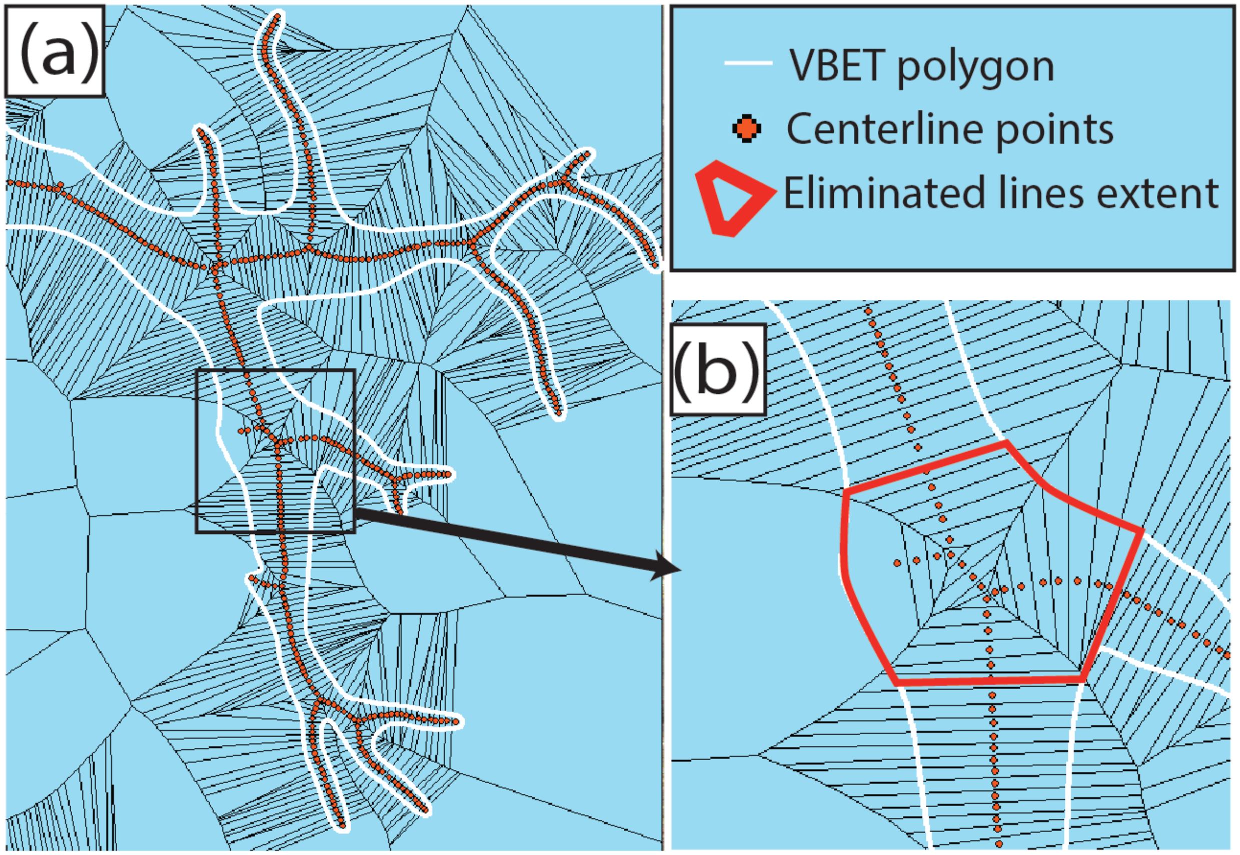

Figure S2 (a) Thiessen polygons (black) around centerline points (red). In step 2, the polygons are maintained only within the VBET boundaries (white). (b) In step 3, intersecting edges of Thiessen polygons are eliminated (e.g., within the red polygon area).

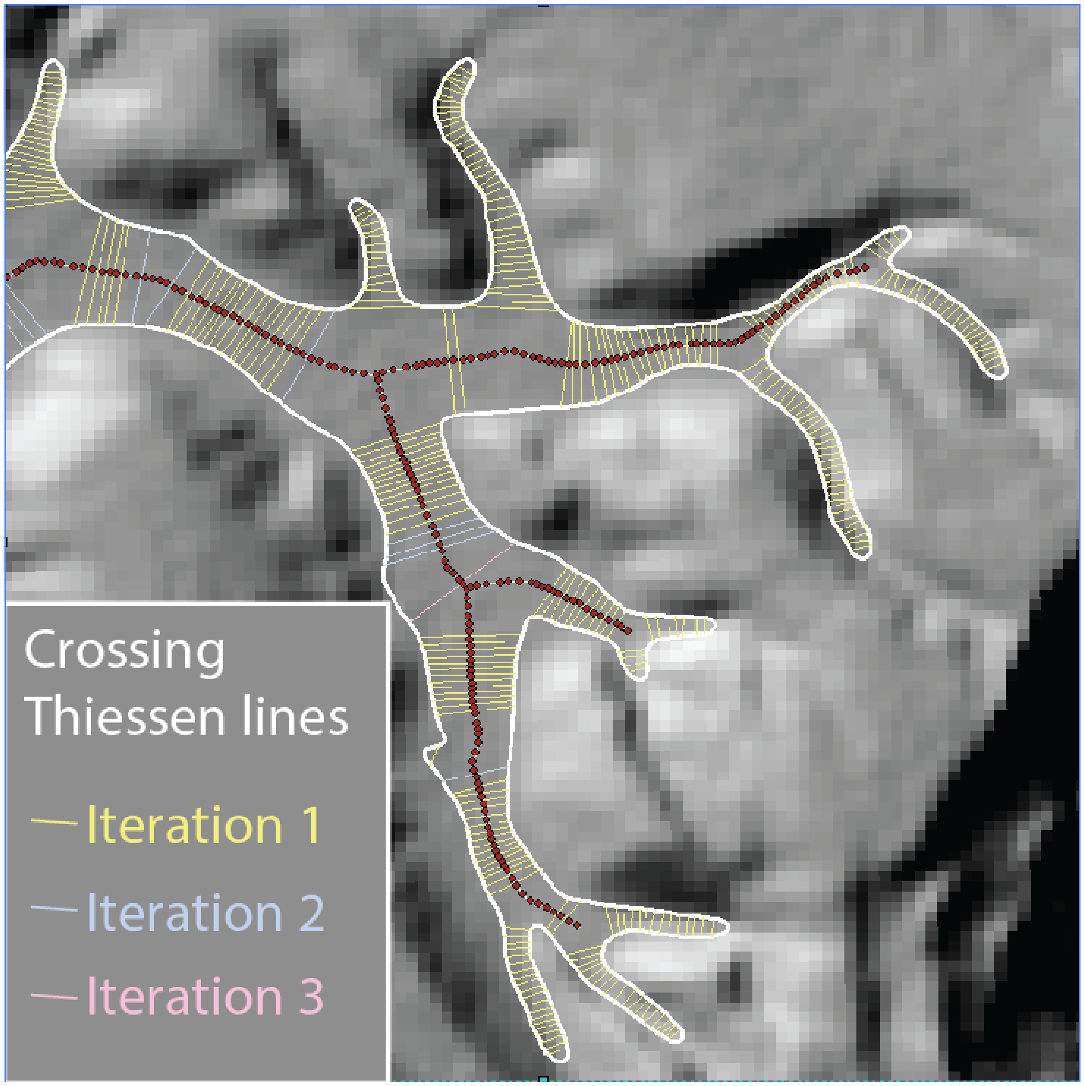

Figure S3: 'Crossing Thiessen lines' compiled from the three iterations described in step 4.

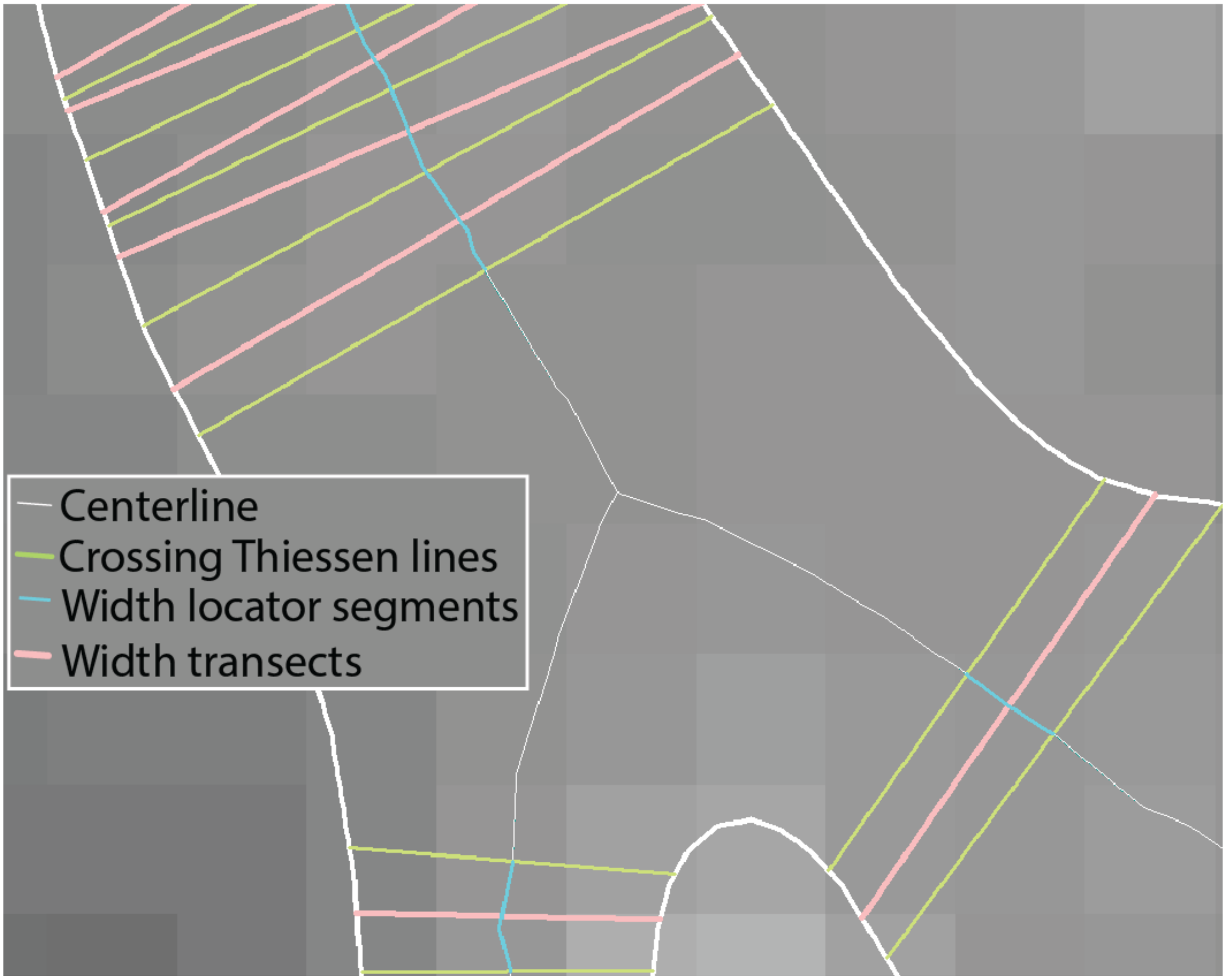

Figure S4: 'Width locator segments' (turquoise) are defined between pairs of originally adjacent 'Crossing Thiessen lines' (Green). Then, 'Width transects' (pink), whose lengths represent the valley width, are generated perpendicular and at the midpoints of the 'Width locator segments.'

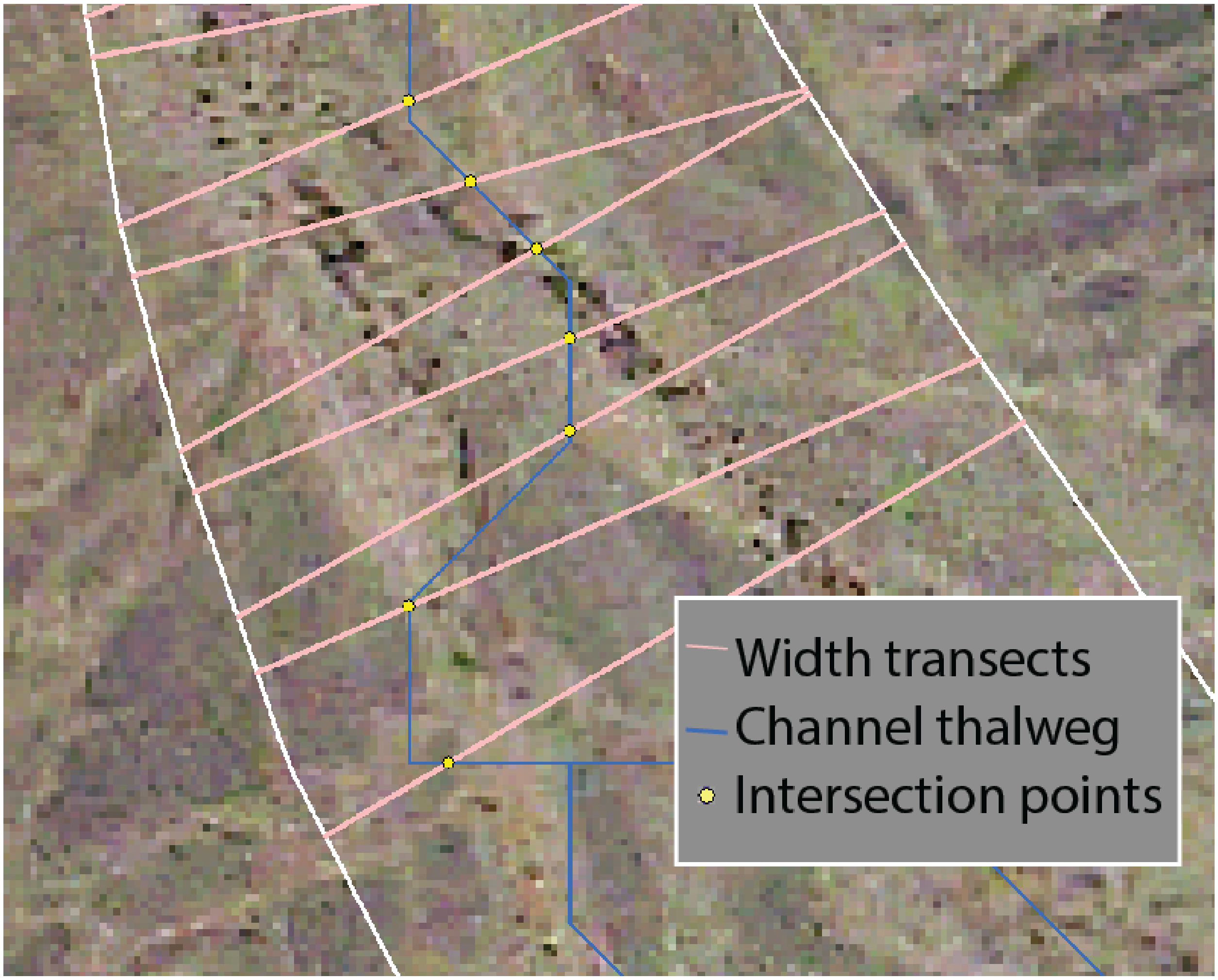

Fig. S5: Intersection points (yellow) are defined along intersections between 'Width transects' (pink) and the thalweg (blue), as part of step 6, illustrated on a 0.5 m resolution orthophoto. In the undisturbed and beheaded flat valleys, the apparent vegetated flow lines (darker pixels) are typically parallel to the valley centerline and not nesseccaraly consistent with the more tortuous DEM-based thalweg (blue).

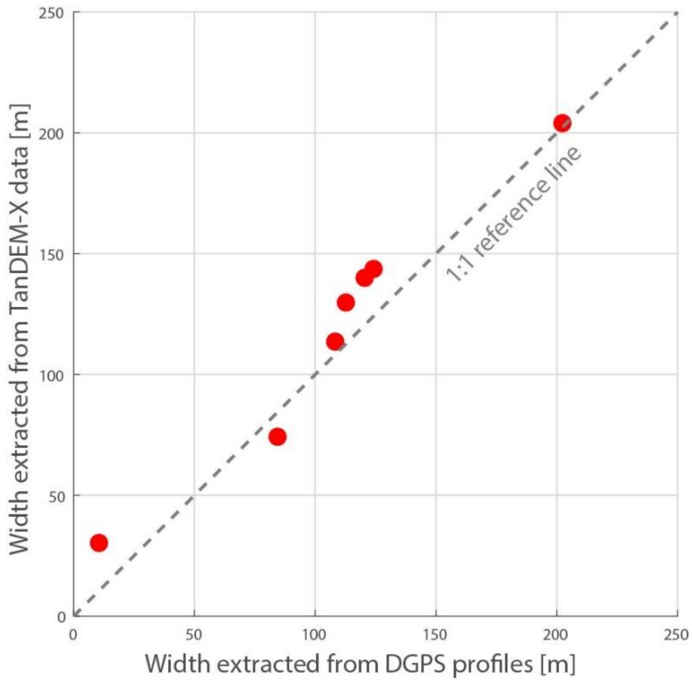

Fig. S6: Comparison of valley width measurements extracted from TanDEM-X and measurements based on differential GPS valley transects. The maximal difference between the measurements is less than 20 m.

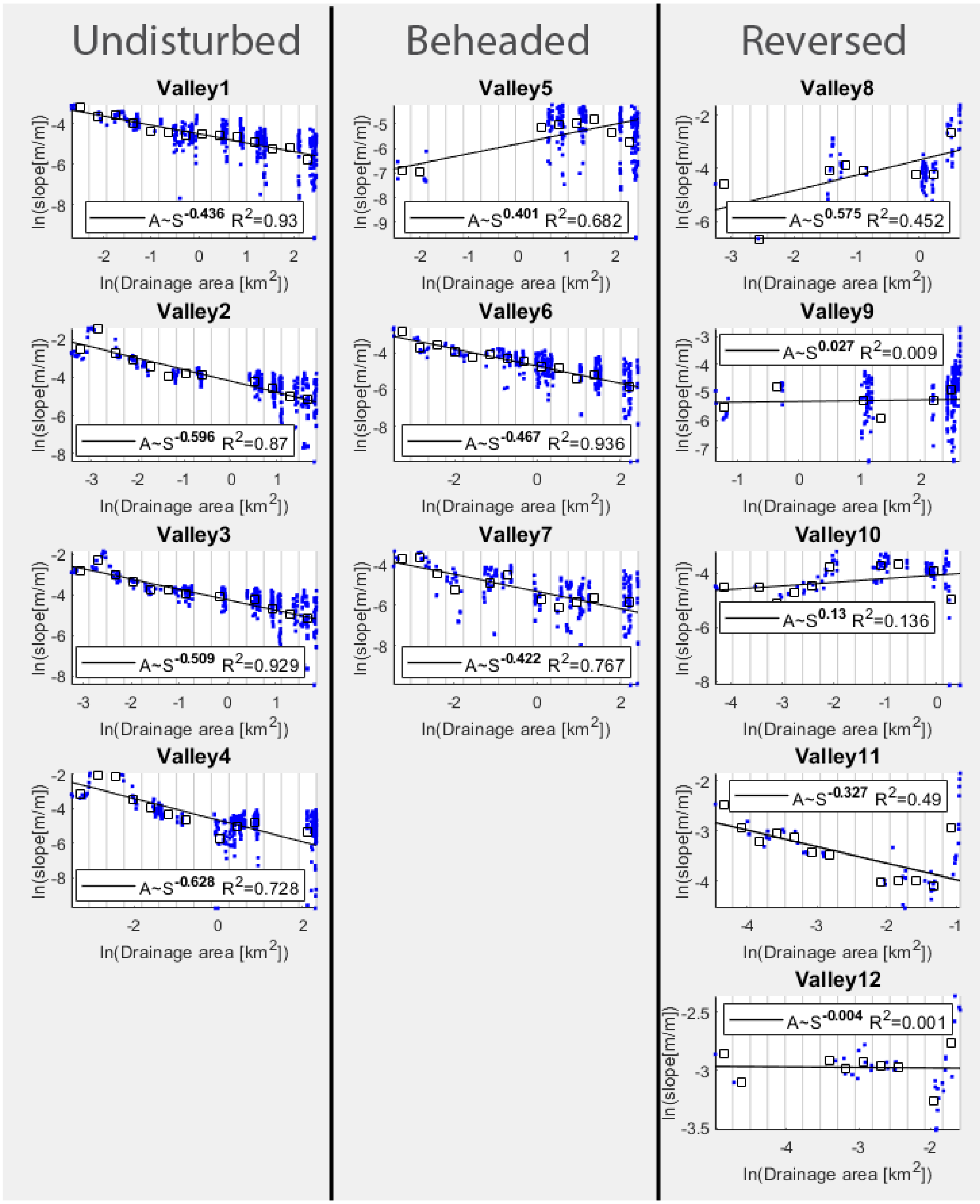

Fig. S7: Best-fit correlations of the slope-area power-law of all valley sections. The regressions were applied to log-binned data (black squares) to reduce the natural noise within the slope data (blue dots).

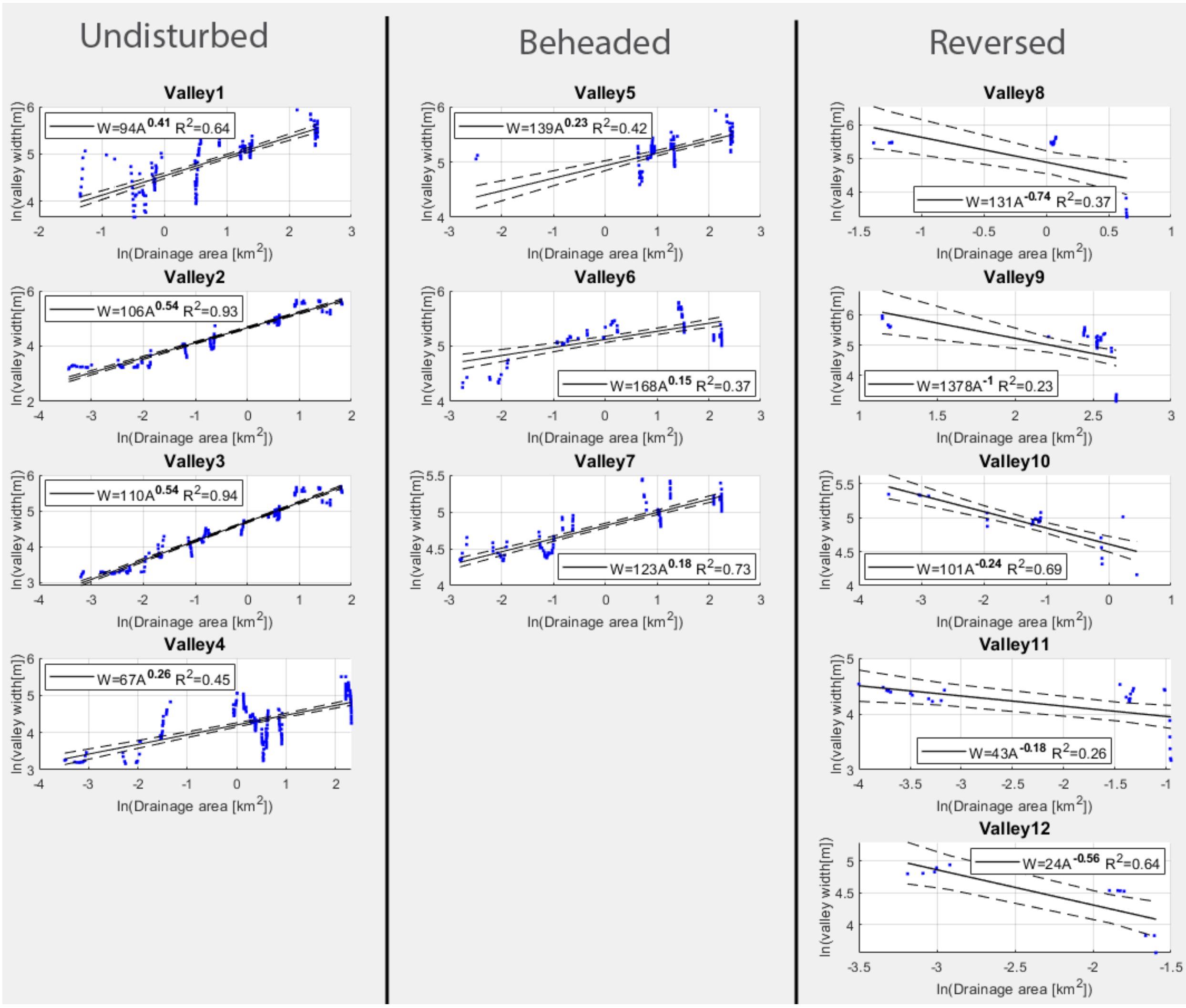

Fig. S8: Best-fits values for valley width-drainage area power law. Blue dots are the raw data, and solid and dashed black lines represent the least-square linear fit and 95% confidence bounds, respectively.

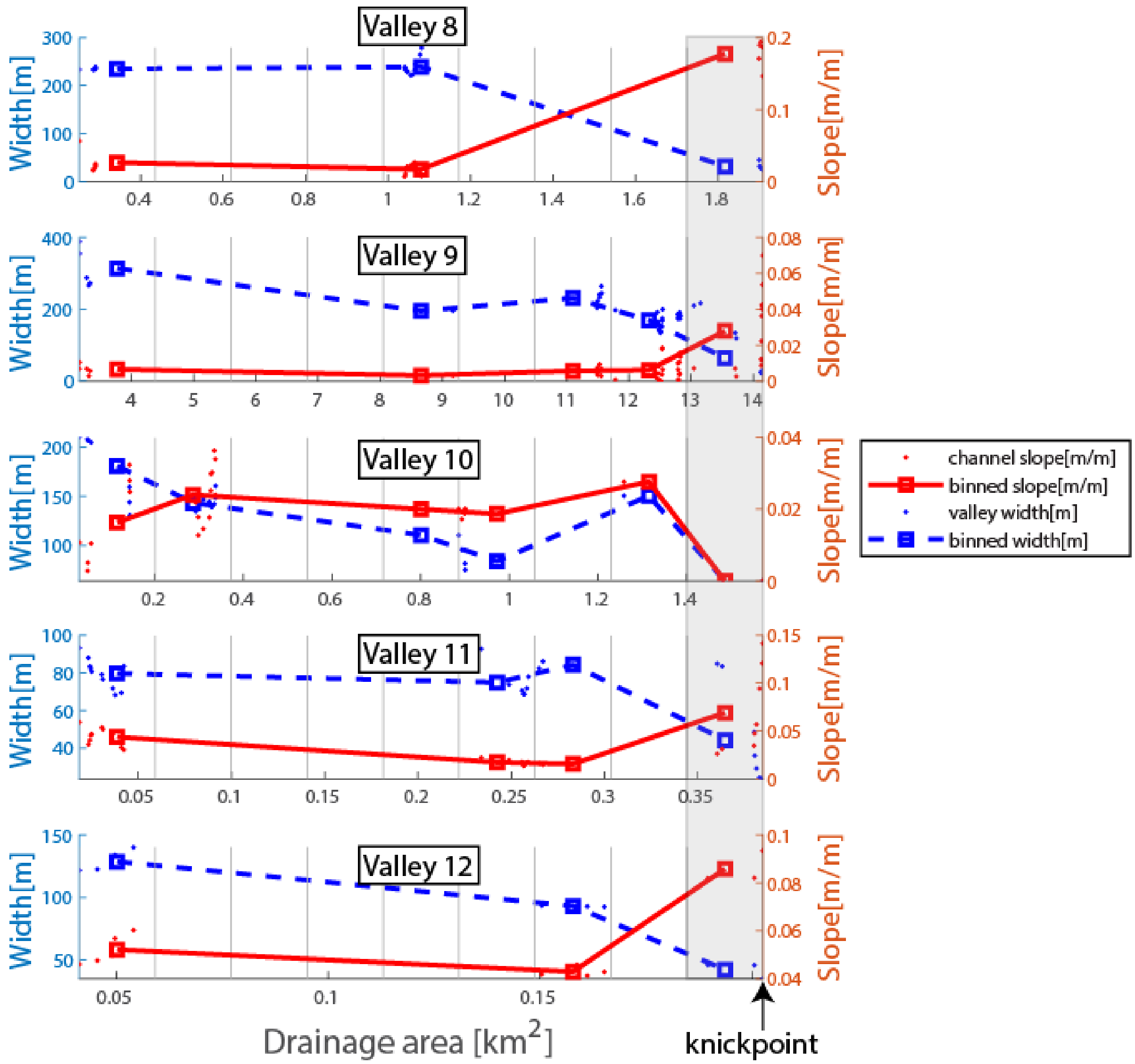

Figure S9 : Slope and valley width (red and blue dots, respectively), plotted against drainage area at the reversed valleys. Excluding valley 10, the valley width narrows, and the slope increases close to the knickpoint (darker area on the right edge of the graphs), such that the two parameters covary. We propose that the observed narrowing and steepening are associated with flow acceleration above the knickpoint lip (Haviv et al., 2010).

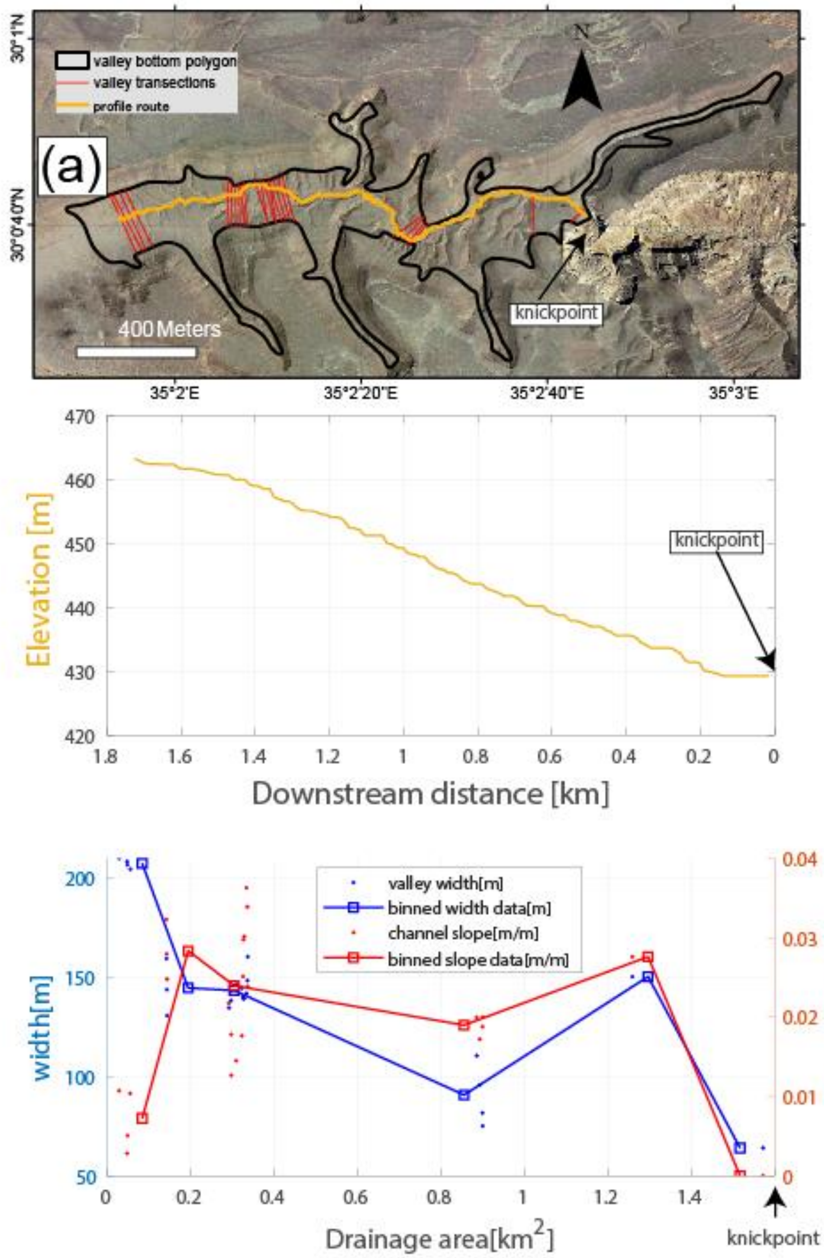

Figure S10. Analysis of the valley width and channel slope in reversed valley 10 (Tables 1 and 2 and Fig. 1d). (a) Valley bottom polygon, valley transects, and a flow pathway of valley 10, on a Orthophoto (0.5m resolution). (b) Elevation profile of valley 10. (c) Valley width (blue) and channel slope (red) vs. drainage area. Here, width and slope do not covary near the knickpoint, unlike the trend of the other reversed valleys in the study area (Fig. S9).

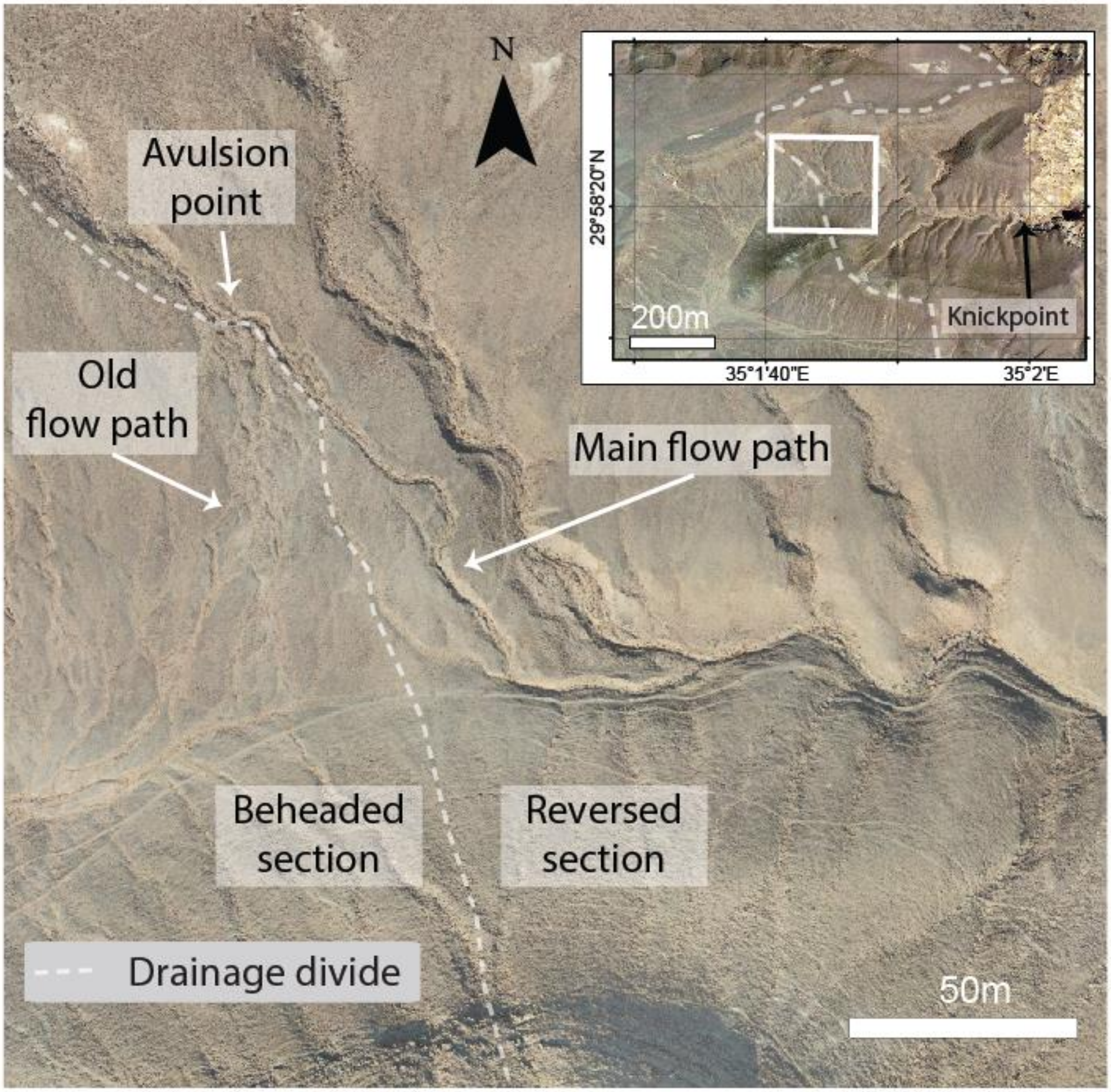

Figure S11. Drone-acquired orthophoto depicting a divergent channel in colluvial fan north of the windgap between the beheaded and reversed sections of valleys 12 and 6, respectively. The remnants of the old flow path suggest that the main flow path used to flow west before it avulsed toward the reversed section. The well-preserved flow traces along the old path demonstrate that it is occasionly active when the main flow path is overflows, suggesting that the avulsion is relatively recent. The inset zoomed-out orthophoto shows the beheaded and the reversed sections across the drainage divide (dashed line) and the spatial extent of the main figure (white rectangle).

Table S1: Parameters used in the ArcGIS tool 'VBET'- valley bottom extractor tool' (Gilbert et al., 2016) for the valleys in the study area

A full description of the VBET parameters is available in:

https://bitbucket.org/jtgilbert/riparian-condition-assessment-tools/wiki/Tool_Documentation/Version_1.0/VBET

Valleys ID	Minimal drainage area of flowlines (pixels)	High drainage area threshold (km^2)	Low drainage area threshold (km^2)	Large slope threshold (degrees)	medium slope threshold (degrees)	Small slope threshold (degrees)	Large Buffer Size (m)	Medium Buffer Size (m)	Small Buffer Size (m)	Aggregation Distance (m)	Degree of manual editing: perimeter (%)[a]	Degree of manual editing: area (%)[b]
1,5	500	3	1	7	6	5	500	400	200	100	0	0
2,3	200	3	1	8	8	6	300	200	200	100	12.5	1.1
4	200	3	1	6	5	4	400	200	200	50	0	0
6,7	200	3	1	8	8	8	1000	500	100	100	0	0
8	200	2	1	8	8	3	400	200	200	100	12.3	2.7
9	500	12	0.1	10	5	3	200	200	400	100	11.5	4
10	50	4	0.1	14	14	14	300	200	200	100	1.1	0.3
11	50	4	0.1	14	14	14	300	200	200	100	10.1	4.7
12	50	3	0.1	6	6	15	300	200	250	50	23.8	9.4

[a]Calculated as: $x = \frac{|\text{polygon perimeter before editing} - \text{polygon perimeter after editing}|}{\text{polygon perimeter before editing}} * 100$

[b]Calculated as: $x = \frac{|\text{polygon area before editing} - \text{polygon area after editing}|}{\text{polygon area before editing}} * 100$

Table S2: Data used for producing Fig. S6, comparing TanDEM-X DEM based valley width relative to DGPS based width measurements.

TanDEM-X DEM based Width (m) [a]	DGPS-based width (m) [b]	Percent deviation, considering measurement errors [c]
30±16	10±1	25.5
74±16	84±1	0
113±16	108±1	0
130±16	113±1	0.3
140±16	119±3	0.2
144±16	124±3	0.3
204±16[d]	202±2	0
RMSE [e] =13m		Mean: 3.7% Std.: 9.6%

[a]The DEM based width measurements were assigned with a constant error of $\sqrt{2}R$, where R=11.6m (section 3.4 in the main text). The error was rounded to 16m.

[b]The DGPS-based width measurements error originate from the uncertainty of the distance between the sampling points along the transect (~1-2m).

[c]Percent deviation is calculated over the minimal difference between the TanDEM-X DEM based and the DGPS based measurements (i.e., widths measurements with overlapping errors are considered to have zero deviation), and calculated as: $\text{Percent deviation} = \frac{|\text{DEM width} - \text{DGPS width}|}{\text{DGPS width}} 100$

[d]In this transect the DGPS measurement generated a profile with two channel bars. Given that the resolution of the TanDEM-X is not sufficient to capture such details, we manually smoothed the elevations across the bars to prevent their identification as the valley boundary.

[e]RMSE is based on the difference between the width extraction measurements without considering errors.

Table S3: P-values of the predictors and for the least-square regressions

Channel ID	k_c coefficient P-value	d exponent P-value	Regression P-value
1	1.40E-197	2.80E-44	2.80E-44
2	1.56E-205	2.31E-91	2.31E-91
3	2.54E-255	1.45E-115	1.45E-115
4	3.02E-250	1.39E-35	1.39E-35
5	8.15E-116	1.14E-14	1.14E-14
6	5.34E-131	3.72E-12	3.72E-12
7	7.85E-192	3.27E-39	3.27E-39
8	2.14E-18	0.002499239	0.002499239
9	5.33E-15	0.000411486	0.000411486
10	6.40E-29	4.30E-07	4.30E-07
11	5.57E-20	0.005935961	0.005935961
12	1.44E-06	0.00188327	0.00188327

Table S4: P-values of the predictors and for the multivariate regressions

Channel ID	k_b coefficient P-value	b exponent P-value	c exponent P-value	Regression P-value
8	7.15E-10	3.76E-03	5.75E-09	3.45E-10
9	1.79E-12	2.23E-04	4.33E-03	3.41E-05
10	1.38E-22	2.70E-07	2.81E-02	3.33E-07
11	3.25E-09	3.19E-08	1.39E-09	1.92E-10
12	9.42E-02*	1.92E-04	3.60E-04	1.33E-05

* Unlike linear regressions where P>0.05 indicates that the predictor predicts no better than a value of 0, in this log-transformed based regression, P-value >0.05 for the coefficient indicates that in a drainage area of 1 km^2 and S=1, the width is not necessarily different from 1m. Additionally, the values of k_b and their P-values depend on the units selected for A (i.e., m^2 or km^2) and W (i.e., m or km). Thus, in that case the P-value >0.05 for k_b is not treated as indicative of insignificant predictor.

References

Dilts, T.E., 2015, Polygon to Centerline Tool for ArcGIS: University of Nevada Reno, http://www.arcgis.com/home/item.html?id=bc642731870740aabf48134f90aa6165.

Gabrish, G., 2020, Create Perpendicular Lines for ArcGIS.:, https://github.com/ShuksanGeomatics/Create_Perpendicular_Lines_ArcGIS.

Gilbert, J.T., Macfarlane, W.W., and Wheaton, J.M., 2016, The Valley Bottom Extraction Tool (V-BET): A GIS tool for delineating valley bottoms across entire drainage networks: Computers and Geosciences, v. 97, p. 1–14, doi: 10.1016/j.cageo.2016.07.014.

Haviv, I., Enzel, Y., Whipple, K.X., Zilberman, E., Matmon, A., Stone, J., and Fifield, K.L., 2010, Evolution of vertical knickpoints (waterfalls) with resistant caprock: Insights from numerical modeling: Journal of Geophysical Research: Earth Surface, v. 115, doi: https://doi.org/10.1029/2008JF001187.

Wessel, B., 2016, TanDEM-X Ground Segment – DEM Products Specification Document: EOC, DLR, Oberpfaffenhofen, Germany, Public Document TD-GS-PS-0021, Issue 3.1, https://tandemx-science.dlr.de/.